Applied Surface Science Advances 30 (2025) 100875

Contents lists available at ScienceDirect

Applied Surface Science Advances

journal homepage: www.sciencedirect.com/journal/applied-surface-science-advances

Full Length Article

Suitable boron-doped graphene substrate for glucose Raman signal enhancement

Jan Komeda [a],*, Antonio Cammarata [a],*, Tomas Polcar [a]

[a] Department of Control Engineering, Faculty of Electrical Engineering, Czech Technical University in Prague, Karlovo Namesti 13, Prague 2, 12135, Czech Republic

ARTICLE INFO

Keywords:
Graphene
SERS
Ab initio
Boron
Glucose

ABSTRACT

Surface-enhanced Raman spectroscopy (SERS) is a highly sensitive and selective technique. It greatly enhances the signal of an analyte compared to classical Raman spectroscopy, due to analyte–substrate interactions. A promising substrate for SERS is boron-doped graphene (B-graphene). At low boron concentrations of ~1.39 at.%, it has been shown to enhance the Raman signal of simple organic molecules such as pyridine. The potential use of high-concentration B-graphene materials for SERS remains unexplored. Therefore, in our study, we investigate the influence of dopant concentration and relative adsorbate/substrate geometry on the effectiveness of B-graphene as a SERS substrate, with glucose as the analyte. We perform Density Functional Theory simulations using the PBE functional and the DFT-D2 van der Waals correction. By combining analysis of interatomic force constants and phonon eigenvector composition, we conclude that higher doping concentrations provide a larger enhancement to the Raman signal of glucose, while the molecule's orientation relative to the surface plays a fundamental role in the Raman response. We suggest that 12.5 at.% B-graphene represents a potential substrate for SERS-based detection of glucose. Additionally, the phonon-based analysis can be promptly applied in the search for promising substrate materials for enhanced Raman response.

1. Introduction

Surface-enhanced Raman spectroscopy (SERS) is a highly sensitive and selective technique; it greatly enhances the signal of an analyte, compared to classical Raman spectroscopy, due to analyte–substrate interactions [1]. A potential application of SERS is the development of novel chemical sensors; a relevant example is the ongoing research into SERS-based glucose sensors [2] for testing patients with diabetes. Compared to typical electrochemical sensors, SERS-based sensors could be used to measure glucose levels from much smaller blood volumes [3] or different bodily fluids, like sweat or the interstitial fluid of skin, with the advantage of being less invasive than current devices.

The most commonly used SERS substrates are noble metals, as they usually provide the largest Raman signal enhancement; however, they have drawbacks such as poor glucose adsorption on bare surfaces [4], high cost, adverse metal–adsorbate interactions, catalytic and photobleaching effects [1]. Significant effort has been put into the research of alternative substrates, especially 2D nanomaterials such as graphene [5], transition metal dichalcogenide monolayers, and Janus structures [1]. Advantages of graphene-based substrates over other 2D materials include their ability to suppress fluorescence [1], simpler atomic structure to synthesize compared to more complex layered materials like transition metal dichalcogenides [6] or MXenes [7], and easy adaptation to several kind of adsorbates [8,9].

In this study, we examine B-graphene as a substrate for glucose detection using quantum mechanical simulations and phonon decomposition analysis. The ideal dopant species and concentration to optimize graphene (or composite materials that include graphene) for a specific application are common topics of interest [10–14]. We aim to build upon this body of research and find doped-graphene materials better suited for application in SERS-based sensing. B-graphene has been shown to enhance the Raman signal of a simple analyte like pyridine by a factor of 10^3 to 10^4 [15,16]; such enhancement is significantly greater than that provided by graphene, which ranges from 2 to 17 [1]. However, these studies have only considered low doping concentrations and non-periodic boundary conditions.

We would like here to stress two aspects concerning the choice of our models. Previous studies have investigated the extent to which graphene can be doped with various atomic species. Researchers utilized different approaches such as the synthetic growth concept (SGC) [17], MD simulations exploring thermodynamic stability [18] or atom intercalation in truncated fullerene-like systems [19]. The recent article by Chaban et al. [18] suggests that B-graphene can remain thermodynamically stable when doped with significantly higher concentrations

* Corresponding authors.
E-mail addresses: komedjan@fel.cvut.cz (J. Komeda), cammaant@fel.cvut.cz (A. Cammarata).

https://doi.org/10.1016/j.apsadv.2025.100875
Received 23 July 2025; Received in revised form 24 September 2025; Accepted 9 October 2025
Available online 16 October 2025

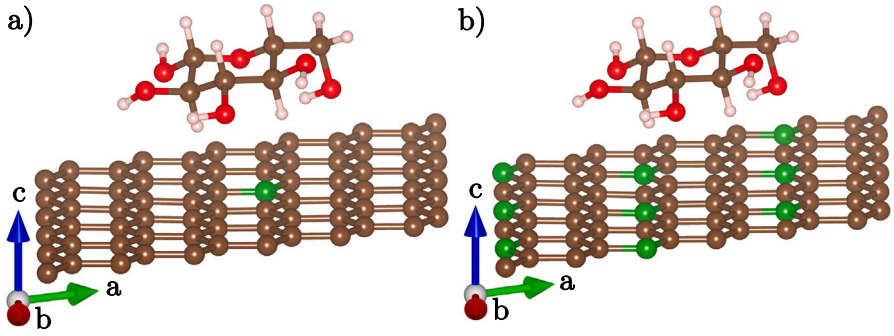

Fig. 1. Initial geometries of the studied systems (a) gLowBG, glucose on ~1.39 at.% B-graphene, (b) gHighBG, glucose on 12.5 at.% B-graphene. Brown spheres represent carbon atoms, while red, white and green spheres represent oxygen, hydrogen, and boron atoms, respectively.

of boron than previously observed. Their claims are supported by current experimental research from Bhushan et al. [20], who have successfully produced a sample of ~19 at.% concentration B-graphene. The "1B" configuration from the work by Chaban et al. has the second highest electric dipole moment. Unlike the configuration with the highest dipole moment, it remains thermodynamically stable at the simulated temperatures of 300, 500, and 1000 K. We choose to specifically study this "1B" configuration, hereafter referred to as the 12.5 at.% B-graphene configuration, because a large electric dipole moment generally contributes to a higher SERS enhancement [1]. High-concentration B-graphene materials have not yet been explored as potential SERS substrates, and as such, they warrant further investigation. Another aspect of our models is the use of periodic boundary conditions. Finite-size geometries in the computational model may introduce severe approximations resulting in poor estimations of the substrate response. When the adsorbate is mostly located far from the boundaries of the substrate, the latter should be modeled as a periodic structure and not as a flake; this is the usual case in experiments, as the spatial extension of the adsorbate is much smaller than typical sizes of graphene substrates [21]. In addition, when graphene flakes are used as a geometric model, the flakes are usually terminated with hydrogen atoms for stability [16,22–25], which introduces fictitious interactions not present in the real system. Lastly, to the best of our knowledge, no computational study on interactions between glucose and B-graphene exists.

For these reasons, the goal of the present work is to explore the effects of different concentrations of boron in B-graphene on the enhancement of the Raman signal of glucose. We are aware of the fact that introduction of dopant atoms into graphene might generate several defects; most common examples include the generation of carbon vacancies or Stone–Wales defects [26–28]. However, simulation of defects formation requires extensive calculations, they then constitute the subject of a study per se, while the focus of the present work is to investigate how the dopant concentration specifically affects the Raman enhancement of the adsorbate signal. We show that 12.5 at.% concentration B-graphene provides a large enhancement to the Raman signal and, as such, it might be better suited as a SERS substrate for glucose sensing. We also discuss how the relative orientation of the molecule with respect to the surface affects the Raman response. Our phonon-based analysis is general and can be promptly applied to the prediction and characterization of Raman signals in the presence of substrates, regardless of the chemical composition of analyte and substrate.

2. Computational details

We select β-glucose as analyte, as it is the most prominent anomer in aqueous solutions (e.g. blood) [29]; the reference atomic geometry is the conformer $^4C_1$ [30]. The graphene layer is placed in the $(\boldsymbol{a}, \boldsymbol{b})$ plane of the unit cell, with the $\boldsymbol{c}$ lattice vector orthogonal to the plane and length set to 50 Å, providing a vacuum slab large enough to avoid any interactions between replicas arising from the periodic treatment of the unit cell. The substrate is modeled by a $6 \times 6 \times 1$ graphene supercell, on top of which we place the glucose molecule with its hydroxymethyl (i.e. CH_2OH) group pointing towards the substrate. This is our reference system, which we name gG (glucose on Graphene). We then modify the gG system by substituting carbon atoms of the graphene layer with 1 and 9 boron atoms, thus creating the gLowBG and gHighBG systems, respectively, the latter consistent with the reported stable geometry [18] (Fig. 1).

Table 1
Structural comparison among the gG structures relaxed by using different vdW corrections. The RDF dot product is calculated between the gG reference system and the same relaxed with different vdW correction; by definition, this amounts to 1 in the "DFT-D2" column, as the structure is compared with itself. The "oxygen-substrate distance" [Å] is the distance measured between the oxygen in the hydroxymethyl group and its closest atom in the substrate.

vdW correction	DFT-D2	DFT-D3	rVV10	optB88-vdW
RDF dot product	1.000	0.997	0.997	0.997
Oxygen-substrate distance	3.140	3.228	3.135	3.123

The graphene layer in gLowBG and gHighBG systems has a boron concentration of ~ 1.39 at.% and 12.5 at.%, respectively.

We perform ab initio calculations within the density functional theory (DFT) framework, as implemented in the VASP software [31]. We use the Perdew–Burke–Ernzerhof energy functional [32] together with the vdW-DFT-D2 van der Waals correction [33], as suggested by previous studies [34,35]. To test our choice of vdW correction against DFT-D3 [36] and nonlocal vdW functionals rVV10 [37] and optB88-vdW [38], we perform additional simulations. Specifically, we relax the gG structure using each option. We compare the relaxed structures to our reference (gG relaxed with the PBE functional and DFT-D2 correction) by computing their radial distribution functions (RDFs) dot products for each possible atomic pair. The RDFs dot products compare all the interatomic distances between all atoms of two structures; we calculate it using the MAISE software package [39]. A value of 1 then means a perfect match and values close to 1 indicate that two structures are very similar. This analysis shows that the resulting geometries are nearly identical (Table 1), with the RDF dot products being always at least 0.997. Additionally, the distance of the oxygen in the glucose hydroxymethyl group from the closest atom in the substrate does not differ from our reference by more than 0.1 Å in any of the structures relaxed with different vdW corrections. According to these findings, we do not expect significant differences in our results if we use any of the tested vdW corrections.

Based on our benchmarks, we set the energy cutoff of the plane-wave basis set to 520 eV and the convergence criterion for the electronic self-consistent field procedure to 10^{-8} eV, while the reciprocal

Table 2
Charge transfer [number of electrons] on the glucose molecule in each system; positive numbers indicate acquisition of electrons of the glucose molecule from the substrate.

System	gG	gLowBG	gHighBG	gLowBGF	gHighBGF
Charge difference	0.14	0.14	0.12	0.13	0.14

space sampling is performed with a maximum of 7 × 7 × 1 Monkhorst–Pack mesh [40]. In all systems including a glucose molecule adsorbed on top of the substrate, the length of the lattice parameters ***a*** and ***b*** correspond to a 6 × 6 × 1 supercell of the primitive graphene cell. Geometric optimization of the pristine graphene model is performed by varying atomic positions together with lattice parameters ***a*** and ***b***, while keeping the ***c*** lattice vector fixed. For all the other models only atomic positions are relaxed while the lattice parameters are held fixed; we make this choice because we assume that the substrate is adhered on a rigid surface for practical applications.

All the model geometries are relaxed until force components on the atoms are less than 10^{-3} eV/Å. The geometry of the optimized structures is reported in the Supporting Information. Second-order force constants are calculated by means of Density Functional Perturbation Theory, and postprocessed with the aid of the PHONOPY [41] software. Raman spectra are evaluated by computing high frequency dielectric tensors at atomic geometries displaced along the Raman active phonon modes as reported in Ref. [42] with the aid of the PHONOPY-SPECTROSCOPY processing tool.

3. Results and discussion

3.1. Geometry optimization

We provide the POSCAR files of relaxed geometries for all studied glucose/substrate systems in the Supplementary Material, section I.

In the relaxed gG system (Fig. 2), the binding distance of 3.140 Å between the oxygen of the glucose hydroxymethyl group and its closest substrate atom agrees with previous studies of glucose adsorption on graphene [43]. A similar bond length of 3.116 Å is realized in the gLowBG case. However, in the gHighBG system, glucose bonds with the substrate at a much shorter distance of 1.684 Å.

Our charge analysis shows only a small transfer of charge from the substrate to the glucose molecule in all systems (Table 2). We perform it by first taking the relaxed geometry of each system, fixing the atoms and calculating the electronic density. We then create two additional systems from each geometry by removing either the substrate or the glucose molecule and again calculate the electronic density without relaxing the atomic positions. In this way, the resulting charge difference originates only from the glucose/substrate interactions, not from the movement of the atoms due to the relaxation process. To assign charge to specific atoms, we utilize the Bader charge analysis [44]. The reported charge difference is then calculated as the total number of electrons of all atoms belonging to glucose in the glucose-on-substrate system minus the total number of electrons of the corresponding lone-glucose system.

In the gHighBG case, we observe that positive charge difference is mainly located in the region between the oxygen of the glucose hydroxymethyl group oxygen and the closest boron atom in the substrate, while negative charge difference is mainly found in the inner region of the molecule and close to the same boron atom (yellow and blue isosurfaces in Fig. 3, respectively). This indicates that once the glucose molecule and the substrate interacts, a shift of charge occurs from the substrate and the molecule towards the hydroxymethyl oxygen and along the axis between the latter and the closest boron atom; by considering the charge difference analysis (Table 2), this amounts to a shift of charge towards the hydroxymethyl group oxygen,

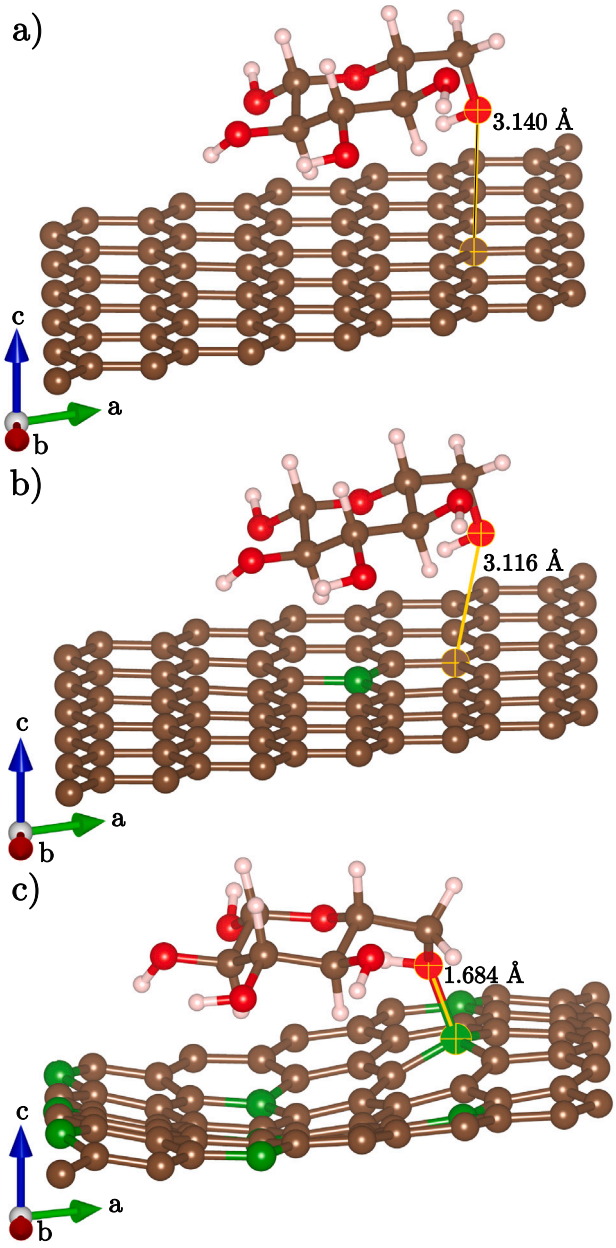

Fig. 2. Relaxed geometries of systems (a) gG (glucose on pristine graphene), (b) gLowBG (glucose on ~1.39 at.% B-graphene) and (c) gHighBG (glucose on 12.5 at.% B-graphene). Bond distances between the oxygen atom of the glucose hydroxymethyl group and its nearest substrate atom are highlighted by yellow lines.

i.e. towards the glucose molecule. Similar behavior is observed for the other systems.

To quantify and compare the effect of the charge transfer on the interaction strength between glucose and substrate in the glucose/substrate systems, we conduct force constant analysis of the glucose hydroxymethyl group oxygen and its closest substrate atom. As the interatomic force constants between two atoms constitute a 3 × 3 matrix, we compare absolute values of matrix traces divided by 3, in order to consider the average magnitude of a force constant on the main diagonal. We consider the trace as a relevant quantity because it remains invariant under spatial transformations of the system coordinates, unlike the full matrix, and thus contains the relevant information on the bond strength. The trace average is found to be ~ 35×10^3 times larger in gHighBG compared to the gLowBG case, indicating a

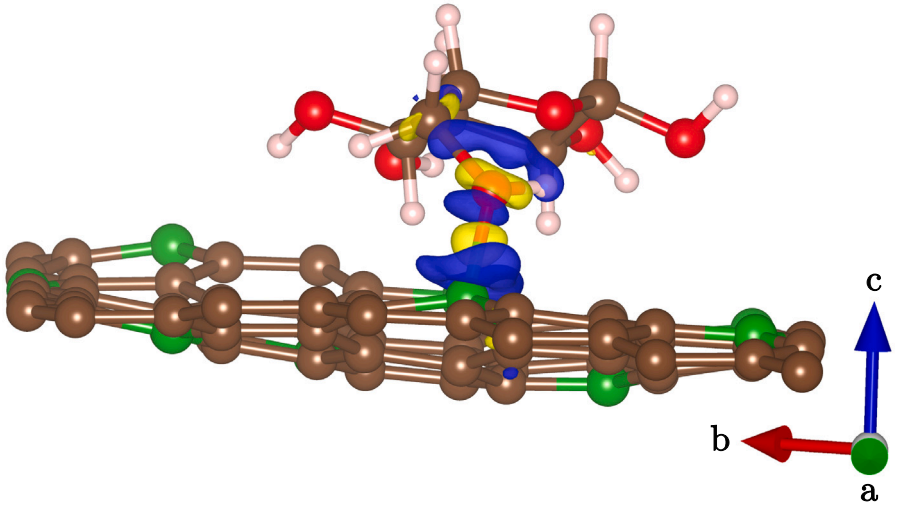

Fig. 3. Charge difference isosurfaces of the gHighBG system. The visualized charge density is calculated as the charge density of the lone glucose and lone substrate systems subtracted from the charge density of the glucose-on-substrate system. The blue and yellow isosurfaces represent loss and gain of charge, respectively. The isosurface levels are set at −0.007 and 0.007 $|e|/\text{Å}^3$, respectively.

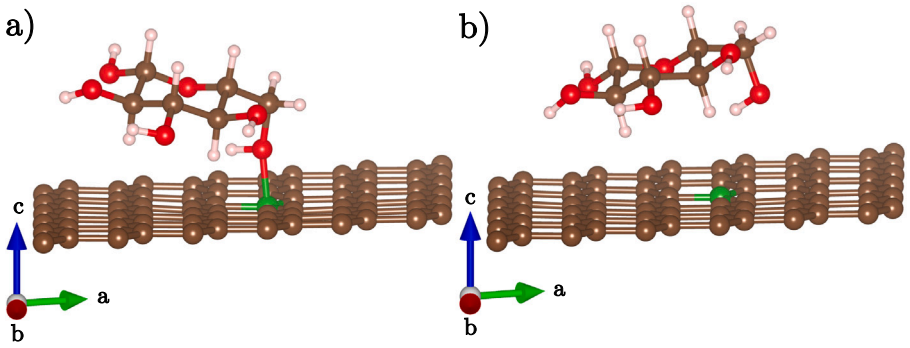

Fig. 4. (a) Initial geometry of a low concentration (∼1.39 at.%) B-graphene system where the CH_2OH group closely interacts with the B site of the substrate. (b) Relaxed geometry of the same system.

much stronger glucose/substrate bond in gHighBG. Instead, the trace average is ∼6 times greater in the gLowBG system compared to the gG one, this pointing at a stronger interaction in the former. However, such difference is significantly lower when comparing the low and high concentration B-graphene systems. The force constant matrices used in this analysis are reported in the Supplementary Material, Section 2.

To check whether a glucose/substrate bond similar in strength to the gHighBG case can form on low concentration B-graphene, we consider the following system, represented in Fig. 4. We position glucose on top of 1.39 at.% B-graphene so that the hydroxymethyl group oxygen is at the same distance from the substrate boron as in the optimized gHighBG system. During geometric relaxation, glucose is repelled to a distance similar to the one found in the gLowBG case. This result suggests that glucose cannot form a strong bond with B-graphene if the dopant concentration is low.

3.2. Phonons and Raman spectra

For all considered systems containing a glucose molecule, the only symmetry operation is the identity; as such, all phonon modes at Γ are Raman active [45]. The frequency range of interest for studying the glucose Raman signal is [600,1600] cm^{-1}, as reported in Ref. [29]. Accordingly, we only compute Raman intensities of modes below 1600 cm^{-1}. Because we are only interested in relative peak positions and intensities, we do not study their temperature-dependent finite width.

First, we calculate the spectrum of pristine graphene as a reference. It consists of a single peak called the G band with a wavelength of 1576 cm^{-1}, corresponding to the first order Raman scattering process, the signal of which is reported to be at ∼1580 cm^{-1} [46]; therefore, we assume that the simulation setup causes a red shift of ∼4 cm^{-1} between the calculated and the expected experimental value. To allow comparison with possible reported experimental data, from now on we report all the calculated spectra shifted by the same amount.

To compare the enhancement of the glucose Raman signal among our systems, we first need to understand which peaks originate from glucose and which from the substrate. We also need to understand which peak in one system corresponds to a given peak in another system (eigenvector comparison). To achieve these two goals, we identify the atomic character of the relevant phonon modes and compare their eigenvectors across the systems. The atomic character quantifies whether the atomic displacement pattern of a mode mainly involves motions of the substrate or the molecule; we calculate it by means of the PHONCHAR code [47]. To establish a one-to-one correspondence between modes originating from the same species, we compare the phonon eigenvectors at varying systems with the aid of the EIGMAP code [48]. Both the PHONCHAR and EIGMAP software packages are available free of charge at https://github.com/acammarat/phtools. Characterization of phonon eigenvectors is necessary to track how the phonon frequency changes under varying conditions; this has been shown, for instance, for the case of the evolution of the Raman signal in transition metal dichalcogenide hetero-bilayers as a function of temperature [48].

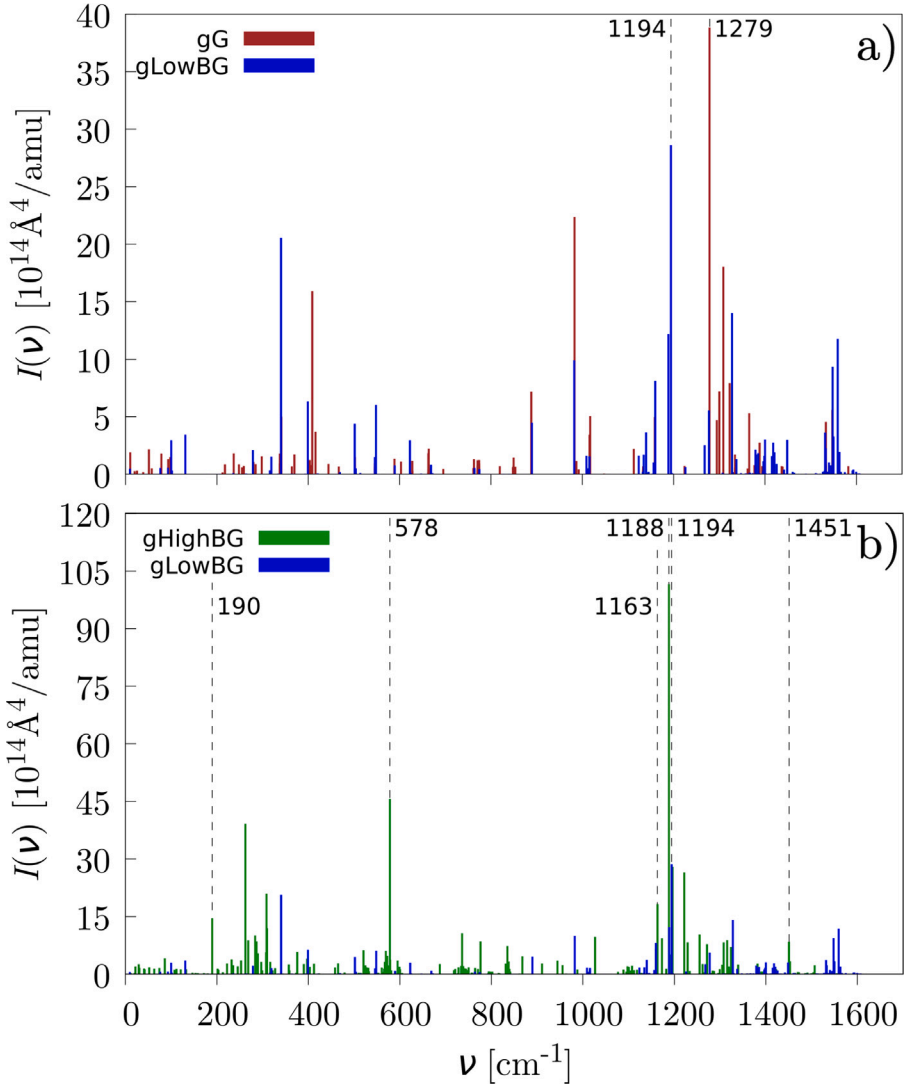

Fig. 5. Raman spectra of (a) gLowBG (glucose on 1.39 at.% B-graphene) and gG (glucose on pristine graphene) systems, and (b) gHighBG (glucose on 12.5 at.% B-graphene) and gLowBG systems. Peaks discussed in the main text are highlighted by dashed vertical lines and labeled with the corresponding wavenumber value.

We now compare the Raman spectra of systems gG with gLowBG and gLowBG with gHighBG (Fig. 5), as this is the central result of the present work. A figure illustrating our phonon character analysis in more detail can be found in the Supplementary Material, Section 3. Thanks to the abovementioned analysis, we determine that in all the glucose/substrate systems, Raman signals in frequency range [870,1350] cm^{-1} originate mainly from the Raman activity of glucose. The peaks in region [1500,1650] cm^{-1} represent the vibrations of graphene and B-graphene in the gG and gLowBG systems, respectively. In gHighBG, peaks corresponding to the vibrations of the substrate appear around 1451 cm^{-1}. By comparing these spectra with the reported spectrum of β-glucose [29] and our calculation of it (see Supplementary Material, Section 4), we see that all substrates enhance the Raman signal of glucose by ~10^{14}, with significant wavelength shifts and modulation of the overall spectra. The most intense glucose peak in the gG system appears at 1279 cm^{-1}, corresponding to the 1277 cm^{-1} peak in gLowBG and 1287 cm^{-1} peak in gHighBG; their relative intensities to the corresponding gG peak are 1.4×10^{-1} and 1.8×10^{-2} for the gLowBG and gHighBG systems, respectively. The latter two peaks are too weak to be clearly visible in the spectrum image. In the B-graphene systems the most intense glucose peaks have frequencies 1194 and 1188 cm^{-1} in gLowBG and gHighBG and correspond to the 1186 cm^{-1} gG peak. Their relative intensities are 1.1×10^4, 3.7×10^4 in gLowBG and gHighBG, respectively. In this instance, the gG peak is not visible. These specific examples illustrate that different peaks become prominent and each mode is shifted by a non-constant factor towards higher or lower frequencies; overall, the 12.5 at.% B-graphene seems to provide the greatest enhancement. A comprehensive list of the most intense glucose peaks and their relative magnitude is provided in Table 1 in the Supplementary Material, Section 4. Special attention should be paid to the peaks at 190 cm^{-1}, 578 cm^{-1} and 1163 cm^{-1} in the gHighBG spectrum. These modes do not correspond to any modes in the other systems as they are peculiar of only the high concentration B-graphene system.

We can qualitatively compare these results to how B-graphene influences pyridine by considering what has been reported in the literature [15]. They concluded that their low concentration B-graphene substrate (~ 2.4 at.%) can increase the SERS signal of pyridine when compared with pristine graphene. This does not seem to be true for glucose. The pyridine molecule was more strongly bonded with the ~ 2.4 at.% B-graphene than pristine graphene, as indicated by a significantly higher adsorption energy. However, in our case there is not much difference in the interaction strength between glucose on pristine graphene or low concentration B-graphene, which could explain why

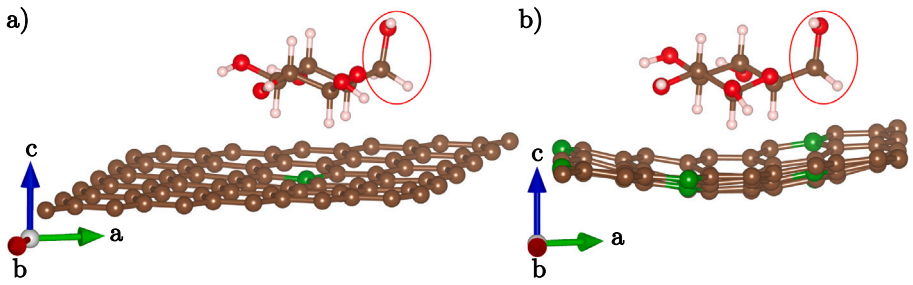

Fig. 6. Relaxed geometries of (a) gLowBGF and (b) gHighBGF systems, where the glucose molecule is flipped; i.e. its hydroxymethyl group, highlighted by a red outline, is pointing away from the substrate.

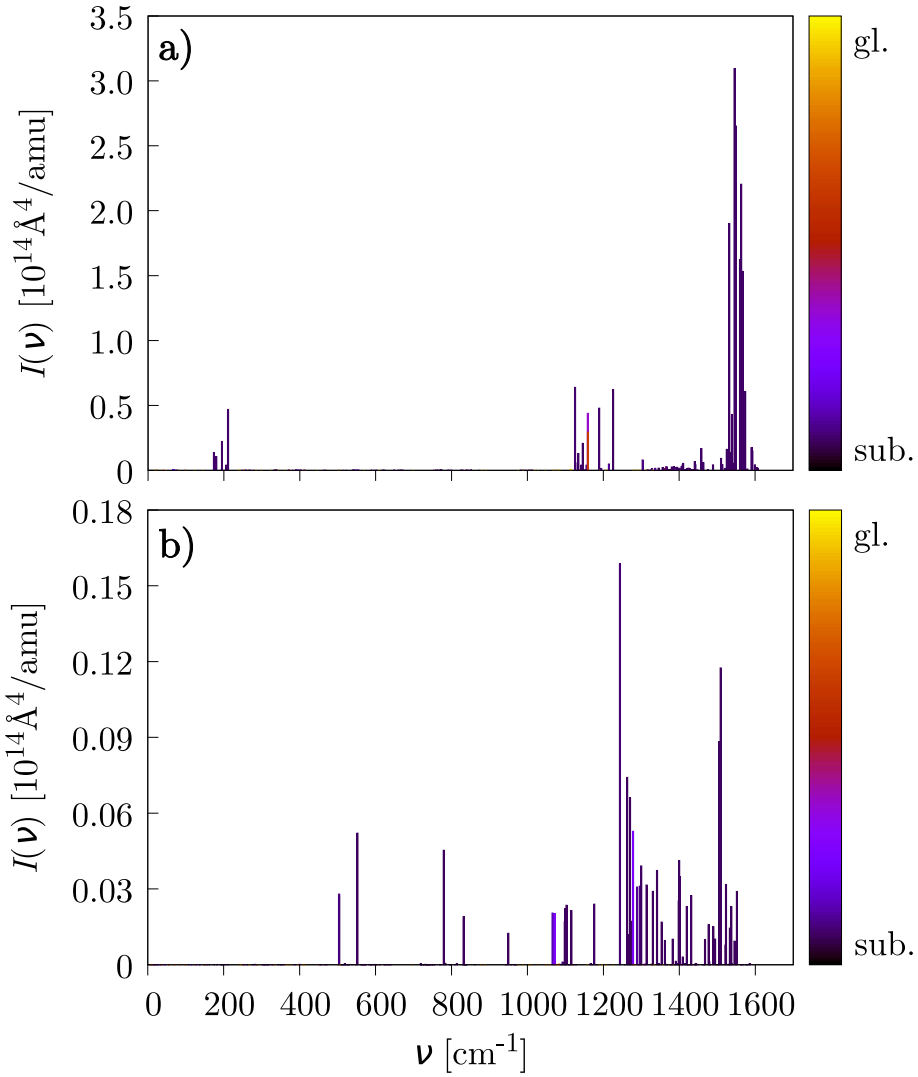

Fig. 7. Raman spectra of (a) gLowBGF and (b) gHighBGF systems. Peak color gradient indicates the atomic character of the phonon displacements: pure yellow and dark purple colors correspond to contributions from only the glucose molecule or the substrate, respectively.

these substrates provide a similar enhancement. In the case of the 12.5 at.% B-graphene there is a significant increase in the interaction strength and, as previously mentioned, it provides the largest signal enhancement. Consequently it may be better suited as a substrate for SERS-based detection of glucose.

To investigate the influence of the hydroxymethyl group's proximity to the substrate on glucose's signal enhancement, we decide to study 2 more systems (Fig. 6), which we name gLowBGF and gHighBGF. They are built by considering the geometry of gLowBG and gHighBG systems and flipping the glucose molecule with the hydroxymethyl group pointing away from the substrate.

Spectra of the gHighBGF and gLowBGF systems (Fig. 7) underline the importance of the proximity of the glucose hydroxymethyl group to the surface in determining the signal enhancement. In both cases, peaks corresponding to substrate vibrations become the most prominent and the Raman signal is overall weaker than in the gHighBG and gLowBG systems. Glucose modes are still present, but weaker by several orders of magnitude than in the non-flipped cases.

4. Conclusion

We have studied the role of dopant concentration in boron-doped graphene when used as a SERS substrate to enhance the Raman signal of glucose. The Raman spectrum of glucose on top of the 12.5 at.% B-graphene substrate exhibited the most intense glucose peaks. This result suggests that 12.5 at.% B-graphene provides a greater signal enhancement than pristine graphene and B-graphene systems with lower concentrations. The large enhancement relates to the substrate's ability to form a stronger bond with glucose compared to the pristine and low concentration cases. We then propose that a dopant concentration of 12.5 at.%, as in the gHighBG system, may be preferable when using boron-doped graphene as a SERS substrate for glucose detection. Additionally, we have found that the orientation of glucose's hydroxymethyl group with respect to the substrate significantly alters the resulting Raman spectrum. The performed phonon eigenvector analysis proved to be fundamental to correctly track the evolution of the Raman signals as a function of dopant concentration. Such analysis can be promptly exploited in other studies on phonon evolution, regardless of the chemical composition and topology of the system of interest.

CRediT authorship contribution statement

Jan Komeda: Writing – review & editing, Writing – original draft, Visualization, Investigation, Formal analysis, Conceptualization. **Antonio Cammarata:** Writing – review & editing, Supervision, Methodology, Funding acquisition. **Tomas Polcar:** Supervision, Funding acquisition.

Declaration of competing interest

The authors declare the following financial interests/personal relationships which may be considered as potential competing interests: Antonio Cammarata reports financial support was provided by European Union. Tomas Polcar reports financial support was provided by European Union. Antonio Cammarata reports equipment, drugs, or supplies was provided by VSB-Technical University of Ostrava IT4Innovations National Supercomputing Center. Jan Komeda reports equipment, drugs, or supplies was provided by VSB-Technical University of Ostrava IT4Innovations National Supercomputing Center. If there are other authors, they declare that they have no known competing financial interests or personal relationships that could have appeared to influence the work reported in this paper.

Acknowledgments

This work was supported by the Ministry of Education, Youth and Sports of the Czech Republic through e-INFRA CZ (ID:90254). The outcomes of this project contribute to the advancement of the project "Robotics and advanced industrial production" (reg.no. CZ.02.01.01/00/22_008/0004590) co-funded by the European Union.

Appendix A. Supplementary data

Supplementary data is provided in a separate pdf file.

Supplementary material related to this article can be found online at https://doi.org/10.1016/j.apsadv.2025.100875.

Data availability

Data will be made available on request.

References

[1] M. Chen, D. Liu, X. Du, K.H. Lo, S. Wang, B. Zhou, H. Pan, 2D materials: Excellent substrates for surface-enhanced raman scattering (sers) in chemical sensing and biosensing, TRAC Trends Anal. Chem. 130 (2020) 115983, http://dx.doi.org/10.1016/j.trac.2020.115983.

[2] X. Sun, Glucose detection through surface-enhanced raman spectroscopy: A review, Anal. Chim. Acta 1206 (2022) 339226, http://dx.doi.org/10.1016/j.aca.2021.339226.

[3] D. Yang, S. Afroosheh, J.O. Lee, H. Cho, S. Kumar, R.H. Siddique, V. Narasimhan, Y.-Z. Yoon, A.T. Zayak, H. Choo, Glucose sensing using surface-enhanced raman-mode constraining, Anal. Chem. 90 (2018) 14269–14278, http://dx.doi.org/10.1021/acs.analchem.8b03420.

[4] K.E. Shafer-Peltier, C.L. Haynes, M.R. Glucksberg, R.P. Van Duyne, Toward a glucose biosensor based on surface-enhanced raman scattering, J. Am. Chem. Soc. 125 (2003) 588–593, http://dx.doi.org/10.1021/ja028255.

[5] S. Chattopadhyay, M.-S. Li, P. Kumar Roy, C.T. Wu, Non-enzymatic glucose sensing by enhanced raman spectroscopy on flexible 'as-grown' cvd graphene, Analyst 140 (2015) 3935–3941, http://dx.doi.org/10.1039/C5AN00546A.

[6] S. Joseph, J. Mohan, S. Lakshmy, S. Thomas, B. Chakraborty, S. Thomas, N. Kalarikkal, A review of the synthesis, properties, and applications of 2d transition metal dichalcogenides and their heterostructures, Mater. Chem. Phys. 297 (2023) 127332, http://dx.doi.org/10.1016/j.matchemphys.2023.127332.

[7] T.A. Oyehan, B.A. Salami, A.A. Abdulrasheed, H.U. Hambali, A. Gbadamosi, E. Valsami-Jones, T.A. Saleh, Mxenes: Synthesis, properties, and applications for sustainable energy and environment, Appl. Mater. Today 35 (2023) 101993, http://dx.doi.org/10.1016/j.apmt.2023.101993.

[8] S.A. Svatek, O.R. Scott, J.P. Rivett, K. Wright, M. Baldoni, E. Bichoutskaia, T. Taniguchi, K. Watanabe, A.J. Marsden, N.R. Wilson, P.H. Beton, Adsorbate-induced curvature and stiffening of graphene, Nano Lett. 15 (1) (2015) 159–164, http://dx.doi.org/10.1021/nl503308c.

[9] D. Solenov, C. Junkermeier, T.L. Reinecke, K.A. Velizhanin, Tunable adsorbate-adsorbate interactions on graphene, Phys. Rev. Lett. 111 (2013) 115502, http://dx.doi.org/10.1103/PhysRevLett.111.115502.

[10] R. Kumar, S. Sahoo, E. Joanni, R.K. Singh, K. Maegawa, W.K. Tan, G. Kawamura, K.K. Kar, A. Matsuda, Heteroatom doped graphene engineering for energy storage and conversion, Mater. Today 39 (2020) 47–65, http://dx.doi.org/10.1016/j.mattod.2020.04.010, URL https://www.sciencedirect.com/science/article/pii/S1369702120301115.

[11] R. Kumar, S. Sahoo, E. Joanni, R.K. Singh, W.K. Tan, S.A. Moshkalev, A. Matsuda, K.K. Kar, Heteroatom doping of 2d graphene materials for electromagnetic interference shielding: a review of recent progress, Crit. Rev. Solid State Mater. Sci. 47 (4) (2022) 570–619, http://dx.doi.org/10.1080/10408436.2021.1965954.

[12] S. Sahoo, R. Kumar, I. Hussain, K. Zhang, Heteroatom doping in 2d mxenes for energy storage/conversion applications, Adv. Powder Mater. 3 (6) (2024) 100246, http://dx.doi.org/10.1016/j.apmate.2024.100246, URL https://www.sciencedirect.com/science/article/pii/S2772834X24000770.

[13] R. Kumar, S. Sahoo, E. Joanni, R. Pandey, W.K. Tan, G. Kawamura, S.A. Moshkalev, A. Matsuda, Microwave-assisted dry synthesis of hybrid electrode materials for supercapacitors: Nitrogen-doped rgo with homogeneously dispersed coo nanocrystals, J. Energy Storage 68 (2023) 107820, http://dx.doi.org/10.1016/j.est.2023.107820, URL https://www.sciencedirect.com/science/article/pii/S2352152X23012173.

[14] R. Kumar, W.C.J. Macedo, R.K. Singh, V.S. Tiwari, C.J.L. Constantino, A. Matsuda, S.A. Moshkalev, Nitrogen–sulfur co-doped reduced graphene oxide-nickel oxide nanoparticle composites for electromagnetic interference shielding, ACS Appl. Nano Mater. 2 (7) (2019) 4626–4636, http://dx.doi.org/10.1021/acsanm.9b01002.

[15] X. Kong, Q. Chen, The positive influence of boron-doped graphene with pyridine as a probe molecule on sers: a density functional theory study, J. Mater. Chem. 22 (2012) 15336–15341, http://dx.doi.org/10.1039/C2JM32050A.

[16] X. Kong, Z. Sun, Q. Chen, The positive influence of boron-doped graphene for its supported au clusters: enhancement of sers and oxygen molecule adsorption, Phys. Chem. Chem. Phys. 14 (2012) 13564–13568, http://dx.doi.org/10.1039/C2CP42297B.

[17] C. Goyenola, S. Stafström, S. Schmidt, L. Hultman, G.K. Gueorguiev, Carbon fluoride, cfx: Structural diversity as predicted by first principles, J. Phys. Chem. C 118 (12) (2014) 6514–6521, http://dx.doi.org/10.1021/jp500653c, URL arXiv:https://doi.org/10.1021/jp500653c.

[18] V.V. Chaban, O.V. Prezhdo, Boron doping of graphene–pushing the limit, Nanoscale 8 (2016) 15521–15528, http://dx.doi.org/10.1039/C6NR05309B.

[19] Intercalation of p atoms in fullerene-like cpx, Chem. Phys. Lett. 501 (4) (2011) 400–403, http://dx.doi.org/10.1016/j.cplett.2010.11.024.

[20] R. Bhushan, A. Bandyopadhyay, S. Kallatt, A.K. Thakur, S.K. Pati, P. Kumar, Microwave graphitic nitrogen/boron ultradoping of graphene, Npj 2D Mater. Appl. 8 (1) (2024) 19, http://dx.doi.org/10.1038/s41699-024-00457-w.

[21] V.B. Mbayachi, E. Ndayiragije, T. Sammani, S. Taj, E.R. Mbuta, A. ullah khan, Graphene synthesis, characterization and its applications: A review, Results Chem. 3 (2021) 100163, http://dx.doi.org/10.1016/j.rechem.2021.100163.

[22] X. Tang, N. Kishimoto, Y. Kitahama, T.-T. You, M. Adachi, Y. Shigeta, S. Tanaka, T.-H. Xiao, K. Goda, Deciphering the potential of multidimensional carbon materials for surface-enhanced raman spectroscopy through density functional theory, J. Phys. Chem. Lett. 14 (45) (2023) 10208–10218, http://dx.doi.org/10.1021/acs.jpclett.3c02962.

[23] G. Faggio, R. Grillo, N. Lisi, F. Buonocore, R. Chierchia, M. Jung Kim, G.-H. Lee, A. Capasso, G. Messina, Nanocrystalline graphene for ultrasensitive surface-enhanced raman spectroscopy, Appl. Surf. Sci. 599 (2022) 154035, http://dx.doi.org/10.1016/j.apsusc.2022.154035.

[24] V. Kaushik, H.L. Kagdada, D.K. Singh, S. Pathak, Enhancement of sers effect in graphene-silver hybrids, Appl. Surf. Sci. 574 (2022) 151724, http://dx.doi.org/10.1016/j.apsusc.2021.151724, URL https://www.sciencedirect.com/science/article/pii/S0169433221027689.

[25] Enhanced sers of the complex substrate using au supported on graphene with pyridine and r6g as the probe molecules, Chem. Phys. Lett. 564 (2013) 54–59, http://dx.doi.org/10.1016/j.cplett.2013.02.006.

[26] E.H. Åhlgren, J. Kotakoski, A.V. Krasheninnikov, Atomistic simulations of the implantation of low-energy boron and nitrogen ions into graphene, Phys. Rev. B 83 (2011) 115424, http://dx.doi.org/10.1103/PhysRevB.83.115424.

[27] L. Tang, S. Shi, C. Yao, S. Zhang, Y. Liu, Z. Duan, J. Jiang, D. Chen, A dft study on defects and n doping to enhance hydrogen storage in mg-decorated graphene, Appl. Surf. Sci. 648 (2024) 159078, http://dx.doi.org/10.1016/j.apsusc.2023.159078.

[28] X.-X. Ma, X. Chen, Y.-K. Bai, X. Shen, R. Zhang, Q. Zhang, The defect chemistry of carbon frameworks for regulating the lithium nucleation and growth behaviors in lithium metal anodes, Small 17 (48) (2021) 2007142, http://dx.doi.org/10.1002/smll.202007142.

[29] C. Araujo-Andrade, F. Ruiz, J. Martínez-Mendoza, H. Terrones, Infrared and raman spectra, conformational stability, ab initio calculations of structure, and vibrational assignment of α and β glucose, J. Mol. Struct.: Theochem 714 (2005) 143–146, http://dx.doi.org/10.1016/j.theochem.2004.09.041.

[30] H.B. Mayes, L.J. Broadbelt, G.T. Beckham, How sugars pucker: Electronic structure calculations map the kinetic landscape of five biologically paramount monosaccharides and their implications for enzymatic catalysis, J. Am. Cheance A Var. DFT-D Funct. Empir. Dispers. Correct. (B97-D, PBE-D, B-LYP-D, BP86-D) Spec. Funct. Treat. Non-Mical Soc. 136 (2014) 1008–1022, http://dx.doi.org/10.1021/ja410264d.

[31] G. Kresse, J. Furthmüller, Efficient iterative schemes for ab initio total-energy calculations using a plane-wave basis set, Phys. Rev. B 54 (1996) 11169–11186, http://dx.doi.org/10.1103/PhysRevB.54.11169.

[32] J.P. Perdew, K. Burke, M. Ernzerhof, Generalized gradient approximation made simple, Phys. Rev. Lett. 77 (1996) 3865–3868, http://dx.doi.org/10.1103/PhysRevLett.77.3865.

[33] S. Grimme, Semiempirical gga-type density functional constructed with a long-range dispersion correction, J. Comput. Chem. 27 (2006) 1787–1799, http://dx.doi.org/10.1002/jcc.20495.

[34] D. Josa, J. Rodríguez-Otero, E.M. Cabaleiro-Lago, M. Rellán-Piñeiro, Analysis of the performance of dft-d, m05-2x and m06-2x functionals for studying $\pi \cdots \pi$ interactions, Chem. Phys. Lett. 557 (2013) 170–175, http://dx.doi.org/10.1016/j.cplett.2012.12.017.

[35] E.G. Hohenstein, S.T. Chill, C.D. Sherrill, Assessment of the performance of the m05–2x and m06–2x exchange–correlation functionals for noncovalent interactions in biomolecules, J. Chem. Theory Comput. 4 (2008) 1996–2000, http://dx.doi.org/10.1021/ct800308k.

[36] S. Grimme, J. Antony, S. Ehrlich, H. Krieg, A consistent and accurate ab initio parametrization of density functional dispersion correction (dft-d) for the 94 elements h-pu, J. Chem. Phys. 132 (15) (2010) 154104, http://dx.doi.org/10.1063/1.3382344.

[37] R. Sabatini, T. Gorni, S. de Gironcoli, Nonlocal van der waals density functional made simple and efficient, Phys. Rev. B 87 (2013) 041108, http://dx.doi.org/10.1103/PhysRevB.87.041108.

[38] J. Klimeš, D.R. Bowler, A. Michaelides, Chemical accuracy for the van der waals density functional, J. Phys.: Condens. Matter. 22 (2) (2009) 022201, http://dx.doi.org/10.1088/0953-8984/22/2/022201.

[39] S. Hajinazar, A. Thorn, E.D. Sandoval, S. Kharabadze, A.N. Kolmogorov, Maise: Construction of neural network interatomic models and evolutionary structure optimization, Comput. Phys. Comm. 259 (2021) 107679, http://dx.doi.org/10.1016/j.cpc.2020.107679, URL https://www.sciencedirect.com/science/article/pii/S0010465520303301.

[40] H.J. Monkhorst, J.D. Pack, Special points for brillouin-zone integrations, Phys. Rev. B 13 (1976) 5188–5192, http://dx.doi.org/10.1103/PhysRevB.13.5188, URL https://link.aps.org/doi/10.1103/PhysRevB.13.5188.

[41] A. Togo, L. Chaput, T. Tadano, I. Tanaka, Implementation strategies in phonopy and phono3py, J. Phys.: Condens. Matter. 35 (2023) 353001, http://dx.doi.org/10.1088/1361-648X/acd831.

[42] J.M. Skelton, L.A. Burton, A.J. Jackson, F. Oba, S.C. Parker, A. Walsh, Lattice dynamics of the tin sulphides sns2, sns and sn2s3: vibrational spectra and thermal transport, Phys. Chem. Chem. Phys. 19 (2017) 12452–12465, http://dx.doi.org/10.1039/C7CP01680H.

[43] P.K. Devi, K. Singh, Electronic and work function-based glucose sensors on graphene, silicene, and germanene sheets – dft studies, Comput. Theor. Chem. 1225 (2023) 114134, http://dx.doi.org/10.1016/j.comptc.2023.114134.

[44] M. Yu, D.R. Trinkle, Accurate and efficient algorithm for bader charge integration, J. Chem. Phys. 134 (6) (2011) 064111, http://dx.doi.org/10.1063/1.3553716.

[45] E. Kroumova, M. Aroyo, J. Perez-Mato, A. Kirov, S.I.C. Capillas, H. Wondratschek, Bilbao crystallographic server : Useful databases and tools for phase-transition studies, Phase Transit. 76 (2003) 155–170, http://dx.doi.org/10.1080/0141159031000076110.

[46] L. Malard, M. Pimenta, G. Dresselhaus, M. Dresselhaus, Raman spectroscopy in graphene, Phys. Rep. 473 (2009) 51–87, http://dx.doi.org/10.1016/j.physrep.2009.02.003.

[47] A. Cammarata, T. Polcar, Fine control of lattice thermal conductivity in low-dimensional materials, Phys. Rev. B 103 (2021) 035406, http://dx.doi.org/10.1103/PhysRevB.103.035406.

[48] A. Cammarata, M. Dašić, P. Nicolini, Integrating Newton's equations of motion in the reciprocal space, J. Chem. Phys. 161 (2024) 084111, http://dx.doi.org/10.1063/5.0224108.